

A DEEP CHANDRA, VLA AND SPITZER IRAC STUDY OF THE VERY LOW LUMINOSITY NUCLEUS OF THE ELLIPTICAL NGC 821

S. Pellegrini¹, A. Siemiginowska², G. Fabbiano², M. Elvis², L. Greenhill², R. Soria^{2,3}, A. Baldi², D. W. Kim²

¹ Astronomical Department, Bologna University, Italy; silvia.pellegrini@unibo.it

² Harvard-Smithsonian Center for Astrophysics, 60 Garden St, Cambridge, MA 02138

³ Mullard Space Science Laboratory, University College London, Holmbury St Mary, UK

Submitted to ApJ

ABSTRACT

The relatively nearby (distance = 24.1 Mpc) elliptical galaxy NGC 821 hosts an extreme example of a quiescent central massive black hole, for which deep Chandra observations revealed a nuclear source for the first time (with $L_{2-10\text{keV}} = L_{\text{Edd}} = 3.6 \times 10^8$). We present here a multiwavelength study of this nucleus, including VLA observations that detect a radio counterpart to the Chandra nuclear source at 1.4 GHz, with a flux density of 127 mJy and possibly a flat spectral shape; we also consider new Spitzer IRAC observations and archival HST images. With these data we discuss possible scenarios for the accretion modalities of the central material that seems available for fuelling, i.e., the stellar mass losses steadily replenishing the circum nuclear region. The final stages of accretion could be radiatively inefficient and coupled to a compact nuclear jet/outflow. The stellar mass losses could instead end up in a standard disc only if a Compton-thick AGN is present. Two extended sources detected by Chandra close to the nucleus could be due to several unresolved knots in a jet. If a jet is present, though, its kinetic energy would be only a very small fraction of the energy associated with the rest mass of the material being accreted. Star formation close to the nucleus is not shown by the available data. Deeper NICMOS, radio and far-IR observations should further constrain the accretion process.

Subject headings: galaxies: elliptical and lenticular, C D { galaxies: individual: NGC 821 { galaxies: nuclei | X-rays: galaxies | X-rays: ISM

1. INTRODUCTION

The connection between the mass of a central supermassive black hole (hereafter MBH) and the properties of the host galaxy (see, e.g., the M_{BH} relation; Ferrarese & Merritt 2000, Gebhardt et al. 2000), together with the recognition that a MBH resides at the center of every massive spheroid in the local universe (e.g., Ferrarese & Ford 2005), has led to the idea that the formation and evolution of the MBH and the host galaxy are intimately related (e.g., Springel, Di Matteo & Hernquist 2005, Sazonov et al. 2005, Hopkins et al. 2006a). In this picture, feedback from the MBH has been advocated to regulate star formation at early epochs, producing the observed galaxy mass function and colors (e.g., Croton et al. 2006); in later epochs, feedback is required to heat the galactic flows solving the "cooling flow" problem (e.g., Omma et al. 2004, Ostriker & Cioffi 2005, Churazov et al. 2005, McDonald et al. 2005).

Although feedback is a promising mechanism for solving many observational puzzles, our understanding of how accretion and feedback work, and of their evolution over cosmic time, is still incomplete. It has been suggested that after the bright AGN phase accretion switches to a more radiatively quiet or inefficient mode (e.g., Churazov et al. 2005, Hopkins et al. 2006b) possibly associated with radio jets or outflows that may carry out most of the accretion power (Di Matteo et al. 2003, Pellegrini et al. 2003, Falcke et al. 2004, Allen et al. 2006). Indeed, the nuclei of most of the nearby spheroids are either radiatively quiescent or exhibit low levels of activity (e.g., Ho 2005, Pellegrini 2005a). Typically, these nuclei are not associated with detectable radio sources, but the absence of radio emission in itself does not ex-

clude nuclear activity, since 'frustrated' or not collimated nuclear outflows would be hard to detect (Nagar et al. 2005). Also, intermittent AGN activity is suggested by the X-ray and radio morphology of nearby clusters of galaxies (e.g., Fabian et al. 2006) and galaxies (e.g., Machacek et al. 2006), and may originate in an accretion flow that switches between different accretion modes (Janiuk et al. 2004).

In nearby spheroids we can attempt to constrain observationally the modalities of accretion (and feedback) through detailed studies of the stellar population, the ISM and the current star formation rate for the central one hundred parsec region, especially if the AGN emission does not dominate over the other nuclear components. NGC 821, an isolated elliptical galaxy at a distance of 24.1 Mpc (Table 1), is an ideal target for studying how these phenomena have evolved in the local universe. There is compelling evidence of the presence of a central MBH in this galaxy, from resolved dynamical studies (Gebhardt et al. 2003). NGC 821 has a very regular and smooth optical appearance (Lauer et al. 2005) and the old and metal rich stellar population typical of elliptical galaxies (Proctor et al. 2005); no cold (H I) or dusty ISM (Sarzi et al. 2006, Ravindranath et al. 2001) have been observed in it, restricting the potential reservoir for accretion.

The MBH of NGC 821 has a mass of $8.5 \times 10^7 M_{\odot}$ (Table 1) and an Eddington luminosity of $L_{\text{Edd}} = 1.1 \times 10^{46} \text{ erg s}^{-1}$. Therefore, if radiatively efficient accretion were taking place, this galaxy should be a luminous AGN. Instead, this MBH is extremely quiescent. Very low limits on optical emission lines (H α , H β , or H γ) are reported for the nucleus of NGC 821 (Ho 2002; Ho

et al. 2003; Sarzi et al. 2006) and the limits on nuclear radio emission are also stringent: < 1.5 mJy at 15 GHz (with 150 m as resolution; Nagar et al. 2005) and < 0.5 mJy at 5 GHz (with 5° resolution; Wrobel & Heeschen 1991).

Thanks to a deep *Chandra* pointing for a total exposure of 230 ksec (discussed in the companion paper Pellegri et al. 2006, hereafter P06), a source was detected for the first time at the nucleus of NGC 821 (called S2). This source has a χ^2 at $(= 1.49^{+0.14}_{-0.13})$ unabsorbed X-ray spectrum, excluding a central concentration of hot, optically thin ISM. S2 is however extended (Tab. 2), therefore an upper limit of 2.8×10^{38} erg s $^{-1}$ was placed on a possible pointlike emission associated with the M BH, one of the smallest obtained with *Chandra* (Pellegri 2005b).

In addition to the nucleus, the hot ISM that could provide a source of fuel for the M BH can be measured in the X-rays (e.g., Loewenstein et al. 2001; Soria et al. 2006a). Our deep, sub-arcsecond *Chandra* pointing revealed diffuse emission in the central part of NGC 821, but also led to the detection of a population of X-ray binaries which can account for most (if not all) of the diffuse emission, so that we could place a very stringent upper limit on the luminosity of a hot gaseous component (P06). This deep pointing highlighted the presence of three other sources around S2, of luminosity and spectral shape typical of low mass X-ray binaries; only one is consistent with being pointlike, the other two (S1 and S4) are extended (Tab. 3), and could be due to the superposition of few point sources and/or truly diffuse emission. In particular, the morphology of S1 resembles a jet-like feature (see also Fabbiano et al. 2004).

In this paper we report the results of an observational campaign aimed at complementing the *Chandra* results, to better constrain the nature of the processes taking place in the vicinity of the M BH in NGC 821. New data presented in this paper include sensitive VLA and Spitzer IRAC observations; we also analyzed archival Hubble Space Telescope (HST) observations. With this multi-wavelength data set we investigate: circum nuclear star formation, which may result from accretion (Tan & Blackman 2005); radiatively inefficient accretion, possibly coupled to a compact or resolved nuclear jet (e.g., Narayan 2005); and highly obscured scaled-down AGN emission. The paper is organized as follows: in Section 2 we summarize the main *Chandra* results concerning the nuclear sources, present the results of the new VLA and Spitzer observations, of the archival HST optical data, and previous N ICMOS results; in Section 3 we discuss possible scenarios for accretion and feedback around this M BH; in Section 4 we summarize our conclusions.

2. THE EMISSION PROPERTIES OF THE NUCLEAR REGION

The main outcomes of the deep *Chandra* pointing concerning the properties of the nuclear source S2 are summarized in Sect. 1 and Tab. 2. We also show the source spectrum (Fig. 1) and the results of a spectral fit including fluorescent line emission from cold iron at 6.4 keV (Tab. 2), which produced only an upper limit on the equivalent width of the line. Tab. 3 summarizes the properties of the other two extended sources (S1 and S4) detected by *Chandra* in the nuclear region (see also Fig. 2). Below we present new VLA observations in Sect. 2.1;

the analysis of IR data from a Spitzer program to observe a sample of radiatively quiescent M BHs (P I: Fabbiano) in Sect. 2.2, together with a previous N ICMOS measurement; the reanalysis of archival HST WFPIC 2 data taken with the F555W and F814W filters, and of our previous R-band INT images in Sect. 2.3. Table 5 summarizes the results and Fig. 3 shows them.

2.1. Radio observations

We observed NGC 821 with the VLA of the NRAO¹ at 1.4 GHz in the most extended (A) configuration on 2004 December 31, and at 4.8 and 8.4 GHz in the second most compact (C) configuration on 2005 July 21. We used a 200 MHz instantaneous continuum bandwidth, observing 3C 48 for flux density calibration and J0203+1134 for phase calibration, using standard techniques and the AIPS data reduction package. NGC 821 lies 1.5° from the phase calibrator. Emission limits on systematic position uncertainties were estimated from snapshots images of three quasars (J0204+1514, J0149+0556, and J0242+1101) that lie within 10° of the phase calibrator. The flux density scale was accurate to $< 3\%$ and absolute position measurements were accurate to $0.1''$. We mapped the entire primary beam of the VLA to obtain robust deconvolutions, obtaining noise levels (1 σ) of 20 Jy, 20 Jy, and 17 Jy at 1.4, 4.8, and 8.4 GHz respectively. We adopted variance weighting of (u,v)-data with some down weighting of short baselines (AIPS parameter ROBUST = 0).

We detected a radio counterpart to source S2 at $\alpha_{2000} = 02^{\text{h}} 08^{\text{m}} 21.174$, $\delta_{2000} = 10^{\circ} 59' 41.4''$ at 1.4 GHz (Fig. 2, Tab. 2; Sect. 4.2 of P06 discusses the coincidence of the position of S2 with the HST-recalibrated position of the optical center), with a flux density of 127 Jy (6 σ). Emission was marginally detected at 8.4 GHz (71 Jy; 4 σ), peaking at the same position to within the measurement uncertainty. The noise level at 8.4 GHz was about one and a half orders of magnitude lower than the earlier upper limit obtained at 15 GHz by Nagar et al. (2005). A marginal detection at 4.8 GHz was also possible (80 Jy; 4 σ); in this case the prospective peak lay 2° (or $\frac{1}{2}$ beam width) to the south.

The three flux densities correspond to a power law with spectral index $\alpha = 0.33 \pm 0.04$ (S $_{\nu} \propto \nu^{\alpha}$). The estimated spectral index may be viewed with some caution because it depends on measurements made with very different beam widths. However, we have studied images at 1.4 GHz made with different weighting schemes (e.g., Natural and Uniform) and do not find a significant change in peak signal-to-noise ratio at the location of S2.

No sources were detected at the location of the other *Chandra* sources S1, S3 and S4 in the nuclear region (Sect. 4 in P06; Fig. 2). Therefore, we can place 4 σ upper limits on their emissions of 80 Jy, 80 Jy and 68 Jy respectively at 1.4, 4.8 and 8.4 GHz (see also Fig. 2).

2.2. Infra-red observations

NGC 821 was observed with the Infrared Array Camera (IRAC, Fazio et al. 2004) on board the Spitzer Space

¹ The National Radio Astronomy Observatory is a facility of the National Science Foundation operated under cooperative agreement by Associated Universities, Inc.

Telescope (Werner et al. 2004) on August 21, 2005 for a total of 725.5 s (Program ID 20371). After the standard Spitzer IRAC processing², the four IRAC channels resulted in images at 3.6, 4.5, 5.8 and 8 μm; the central region of NGC 821 was detected in each of them. We based our analysis on the IRAC instrument performance as given in the Infrared Array Camera Data Handbook³.

Using DS9 and funtools⁴, we extracted counts from circular regions of approximately 4 square arcseconds area (1.01 radius) centered on the peak of the emission. In every case the position of this peak, with the Spitzer WCS, falls in-between the optical center and the Chandra position for S2 (see Sect. 4.2 of P06 for more details); both of these are well within the count extraction radius. This position (Spitzer WCS) is at RA = 02^h 08^m 21^s.11, Dec = +10° 59' 42".0, although given the pixelation of the data, the peak count pixel may be slightly displaced.

The background was estimated both from a surrounding annulus, to attempt a rough subtraction of stellar light from the centralmost emission, and from an off-source circle. The fluxes were all normalized to an area of 4 square arcseconds (that of circles of 1.01 radius). The results are shown in Table 4, for both choices of the background.

We also list in Tab. 5 the upper limit on any unresolved nuclear emission in the H-band (centered at 1.6 μm) derived from NICMOS data (Ravindranath et al. 2001). This limit refers to the NIC2 camera and corresponds to an intrinsic Gaussian of FWHM = 0.5 pixel.

2.3. Optical observations

We carried out aperture photometry on the archival HST WFC2 images taken with the F555W and F814W filters (Lauer et al. 2005), following standard procedures described in the web⁵. The instrumental F555W and F814W magnitudes were converted to standard V and I magnitudes using the most updated version of the color coefficients provided by A. Dolphine (see also the web⁶). In order to compare the optical emission with that estimated from Spitzer IRAC observations, it was calculated for a circle of 1.01 radius, the same area used to extract the Spitzer fluxes (Sect. 2.2). The optical brightness inside this area is $V_0 = 15.0 \pm 0.1$ mag, and $I_0 = 13.7 \pm 0.1$, after correcting for a Galactic extinction $E(B-V) = 0.11$ (Schlegel et al. 1998). The R-band magnitude from the same area was also calculated, by using INT images (Graham et al. 2001) and the corresponding surface brightness profile derived by Soria et al. (2006b); it results into $R_0 = 14.3 \pm 0.1$ in the Cousins system.

In order to constrain the emission coming from the MBH, from the deconvolved F555W and V images derived by Lauer et al. (2005) we also calculated the V and I luminosities within a circle of 0.046 radius (the innermost radius at which deconvolution can give accurate results according to Lauer et al.). These luminosities are upper limits to the MBH emission, since both our analysis and that of Lauer et al. (2005) reveal the absence

of an optical "nucleus", that is a compact light source rising above the surface brightness profile at small radii when extrapolated inward. In general these nuclei, which have been found in a large fraction of early-type galaxies from HST images (see also Ravindranath et al. 2001), are bluer than the background starlight and could be nuclear star clusters or low luminosity AGNs.

3. DISCUSSION

The deep Chandra image of NGC 821 revealed an extended, hard source at the position of the galactic center (P06); our associated VLA observations have led to the discovery of a 1.4 GHz source at the same position (Sect. 2.1); nuclear emission is not detected in the optical and the IR (Sects. 2.2 and 2.3). In the 0.3–8 keV band the 3 upper limit to any pointlike emission associated with the MBH is 2.8×10^{38} erg s⁻¹, and the L at 1.4 GHz is just 1.2×10^{35} erg s⁻¹. Therefore the MBH of NGC 821 is one of the radiatively quietest MBH known, with $L_X = L_{\text{edd}} < 2.5 \times 10^{-8}$. Most MBHs are radiatively quiescent in the local universe, or show very low activity levels (Sect. 1), therefore our deep look at the nucleus of NGC 821 has a bearing on a very common state of MBHs. In the following we use our observational results to constrain the process of accretion and feedback in this nucleus.

3.1. Why not a dead MBH?

Given the general lack of fuel available for accretion observed at all wavelengths, including the X-rays (Sect. 1), is a truly dead MBH what we should expect at the center of NGC 821? In fact, an aging stellar population continuously returns gas to the ISM, via its stellar mass losses (Cioffi et al. 1991, David et al. 1991), and the circum nuclear region should be replenished with this fuel. Indeed, hydrodynamical simulations specific for NGC 821 (P06) demonstrate that this fuel should be present. While the bulk of the hot gas is expelled out in a wind (consistent with the lack of detection of hot gas), P06 found that the stellar mass losses are accreting within a very small region of ~25 pc from the nucleus; at the innermost radius resolved by the simulations (10 pc), the mass accretion rate is $M_{\text{in}} = \text{few } 10^{-5} M_{\odot} \text{ yr}^{-1}$. Notwithstanding the limitations of the simulations, and the uncertainties associated with the observables used as input parameters (see P06), the presence of this small inner region was considered a robust result; similarly, a range of values for $M_{\text{in}} = (2-7) \times 10^{-5} M_{\odot} \text{ yr}^{-1}$ was considered reliable (with the caveat that the true, final accretion rate on the MBH could be somewhat higher; P06). M_{in} should produce a luminosity $L_{\text{acc}} = M_{\text{in}} c^2 / (1.4 \times 10^{41} \text{ erg s}^{-1})$ if, closer in to the MBH, it ends up in a standard accretion disc with a radiative efficiency = 0.1 as assumed for classical AGNs (Shakura & Sunyaev 1978). This would be a highly sub-Eddington AGN, though, since $L_{\text{acc}} = L_{\text{edd}} = \text{few } 10^{-5}$. For a standard spectral energy distribution (SED) of AGNs (Elvis et al. 1994), the upper limit on a pointlike nuclear X-ray emission (Tab. 2) corresponds to a bolometric upper limit of $L_{\text{bol}} = 4 \times 10^{39}$ erg s⁻¹, that is 30 to 100 times less than L_{acc} .

Below we explore scenarios for the evolution of the accreting material, that would explain why the nucleus is not observed at a luminosity as high as L_{acc} . We

² http://ssc.spitzer.caltech.edu/irac/dh/PDD_v1.pdf

³ <http://ssc.spitzer.caltech.edu/irac/dh/iracdatahandbook3.0.pdf>

⁴ hea-www.harvard.edu/RD/fintools/

⁵ See http://www.stsci.edu/instruments/wfc2/W_fpc2_hand/w_fpc2_tutorial.pdf

⁶ See http://purcellas.arizona.edu/w_fpc2_calib/.

consider, in turn, the presence of angular momentum in the accreting material (Sect. 3.2), a reduction of the accretion rate due to star formation in a circum nuclear disc (Sect. 3.3), accretion at low radiative efficiency (Sect. 3.4), the presence of a jet/outflow, whose kinetic power possibly accounts for a fraction of $M_{\text{in}} c^2$ and heats the surroundings (Sect. 3.5), a transition in the accretion mode due to disk instabilities (Sect. 3.6), and finally obscuration of the nuclear radiation produced by a scaled-down AGN (Sect. 3.7).

Note that the mass accretion rate of galactic nuclei has been often estimated (e.g., Di Matteo et al. 2003) assuming spherically symmetric accretion from a nonrotating polytropic gas with given density and temperature at infinity (Bondi 1952). Moscibrodzka (2006) calculated model spectra emitted by such a Bondi flow for a sample of low luminosity AGNs, including NGC 821. The adopted value of gas density was larger than constrained now thanks to the deep Chandra pointing (P 06); even so, the predicted X-ray emission was $< 2.6 \cdot 10^{33} \text{ ergs s}^{-1}$, that is 5 orders of magnitude below the limit on point-like nuclear emission (Tab. 2). However, the Bondi accretion is a severe underestimate of the accretion process (see also P 06); for example, some initial angular momentum of the flow captured by the MBH, and the inclusion of viscosity, may result in a higher X-ray luminosity. Radiation models applied to global MHD simulations of low angular momentum accretion flows are being developed and will be applied to this nucleus (Moscibrodzka et al., in preparation; see also Balbus & Hawley 2002).

3.2. Angular momentum at large radii

The inclusion of even slow rotational motion of the gas at large radii can significantly reduce the rate at which mass is captured into the accretion flow, compared to the non-rotating case (Proga & Begelman 2003). The motivation for the Proga & Begelman's study was to make less severe the problem that MBHs in the local universe are much dimmer than expected for a mass accretion rate estimated at large radii via the Bondi (1952) formula (Sect. 3.1) and ending up in a standard disc (e.g., Fabian & Canizares 1988, Pellegrini 2005a). While the Bondi formula assumes spherically symmetric accretion from a nonrotating gas under the sole influence of the central gravity, Proga & Begelman (2003) studied the evolution of the flow with a small angular momentum, including regions beyond the domination of the MBH gravity. They found that the mass supply rate to the MBH can be smaller by up to 2 orders of magnitude with respect to the nonrotating case. In NGC 821 the stellar kinematics becomes disc-like within the central $10''$ (Scorza & Bender 1995, Emsellem et al. 2004), therefore the stellar mass losses close to the galactic center are likely to have angular momentum, which would lead to a reduction of M_{in} .

Whether the expected luminosity could become consistent with the observed upper limits is however more questionable, since it is not known what is the final, net effect of the inclusion of angular momentum at large radii on the resulting luminosity of the flow closer to the MBH. It is probably not plausible that gas is flowing at the rate shown by the simulations (that is equal to M_{in}

of Sect. 3.1 at present and was larger in the past, for a total integrated mass of few $10^6 M_{\odot}$ over the past 10 G yrs; P 06) continues to accumulate form any G yrs in the nuclear region without accreting and without becoming observable. However, in order for the gas to be able to accrete, angular momentum must be transferred outward through viscosity, and this may actually increase the luminosity of the flow. MHD simulations with rotation and cooling by radiation included are needed to really state what happens to the luminosity of the flow (as concluded also at the end of Sect. 3.1).

3.3. Circum nuclear star formation

Condensation into stars in a gravitationally unstable disc can prevent a significant fraction of the accreting gas from reaching the MBH (Tan & Blackman 2005), resulting into a much lower true accretion rate; this star formation should produce H and IR emission. As reported in Sect. 1, the optical spectrum of NGC 821 shows only absorption lines; the 3 upper limit on its H luminosity is $L_H < 1.46 \cdot 10^{38} \text{ erg s}^{-1}$ (Ho et al. 2003, rescaled for the distance in Tab. 1). From the Kennicutt (1998) relation between star formation rate and L_H , the resulting star formation rate is $< 10^3 M_{\odot} \text{ yr}^{-1}$, much larger than M_{in} given by the simulations (Sect. 3.1). Also the observed luminosity in the IRAC bands (Tab. 5, Fig. 3) is at least one order of magnitude higher than expected in the full IR band from star formation at the M_{in} rate (Kennicutt 1998). However, the aperture used to derive the IRAC luminosities includes also emission from the normal, old stellar population, and it could be that M_{in} is so low that the available optical and IR data cannot constrain whether a part (or even the total) of M_{in} goes into star formation.

The analysis of the SED of NGC 821 (Fig. 3) confirms that it can be explained just by the normal, old galactic stellar population, without requiring ongoing star formation. To check this, we used the matched aperture photometry (i.e., all for $1.01''$ aperture radius) from the Spitzer to the V filter data points (Tab. 5) and compared it with SED templates for stellar populations of different ages and metallicities, for the Kroupa (2001) IMF (Bruzual & Charlot 2003); we also allowed for an exponentially declining star formation rate with time scale

. The fitting procedure described by Bolzonella et al. (2003)⁷ was applied. The observed data points are very well fitted by an age of 11.0 G yrs and a metallicity of 0.25 solar, with a short time scale ($\tau = 0.1 \text{ Gyr}$) and without current star formation (solid line in Fig. 3). These properties match closely those obtained from spatially resolved optical spectroscopy for the bulk of the stellar population (Proctor et al. 2005). The magnitudes and fluxes derived here have been corrected for extinction (Sect. 2); to check whether a residual extinction is left in the data, we allowed for free extinction in the fit, but the best extinction turned out to be consistent with zero. We can conclude that the optical and mid-IR emission within a central projected circle of $1.01''$ radius is dominated by the normal stellar population of the galaxy.

⁷ This fitting can be made with the public code hyperz, available on the web at <http://webast.ast.obs-mip.fr/hyperz> and built by Bolzonella et al. (2003).

From their analysis based on Lick absorption-line indices, Proctor et al. (2005) also found at the very center of NGC 821 (within a central radius of $1''$) an emission weighted abundance of 3 times solar, and evidence for a burst of starformation between 1 and 4 G yrs ago, that involved $< 10\%$ of the galaxy's mass. Therefore we fitted the observed data points also with a metallicity of 2.5 solar (the largest value available for the templates); this procedure resulted in an age of 1 G yr, but the fit was not as good as the previous one (dotted line in Fig. 3). The optical points considered here contain less information than the indices used by Proctor et al. (2005); it is also likely that the true best fit SED is a combination of templates with different ages and abundances, but a fit with composite SEDs is beyond the scope of this work. For the purposes of the present investigation, the conclusion here is that current starformation is not required to explain the SED, as also obtained in the different (and likely more sensitive) investigation by Proctor et al. (2005).

3.4. Low radiative efficiency (plus a compact, nuclear jet)

It has been suggested that high-luminosity and low-luminosity AGNs host two different accretion modes: a radiatively efficient disk-dominated one and a radiatively inefficient one, which is expected to be coupled to strong outflows (see Narayan 2005 for a recent review). In the radiatively inefficient mode, the flow produces the X-ray emission, while the radio emission (if present) should come from the base of a nuclear jet (e.g., Falcke et al. 2004, Kording et al. 2006). This picture is supported by the observation of low-luminosity AGNs being "radio-loud" (Ho 2002, Terashima & Wilson 2003, Pellegrini et al. 2003, Wu & Cao 2005); moreover, their radio power and sometimes also their radio spectrum requires a separate, compact jet component (Anderson et al. 2004; Nagar et al. 2005). On the theoretical side, MHD simulations show that at low accretion rates winds and jets naturally develop (e.g., Stone et al. 1999, Hawley & Balbus 2002, Igumenshchev et al. 2003, De Villiers et al. 2003), since the magnetic and kinetic energy release in the flow are enough to support an outflow or a jet (see also Blandford & Begelman 2004).

In this context, the relationship between the black hole mass, the core radio luminosity at 5 GHz and the 2-10 keV emission has been investigated for a large sample of accretion-powered sources, going from X-ray binaries to mostly low-luminosity AGNs (Meroni et al. 2003). They found the sources to lie on a plane described by $\log L_R = 0.60 \log L_X + 0.78 \log M_{BH} + 7.33$ (with a scatter of $\sigma_R = 0.88$), which was attributed to the presence of a radiatively inefficient accretion flow + jet system, that can exist with similar properties at different scales.

Low radiative efficiency accretion is compatible with the very low value of $L_X = L_{Edd} < 2.5 \cdot 10^{-8}$ (Sect. 3) for the MBH of NGC 821, so we examine the position of this MBH with respect to the plane of Meroni et al. (2003). The 2-10 keV upper limit on nuclear pointlike emission is $1.8 \cdot 10^{38} \text{ erg s}^{-1}$ (Tab. 2), and the nuclear 5 GHz luminosity is $2.7 \cdot 10^{35} \text{ erg s}^{-1}$ (a 4.0 detection, though; Sect. 2.1); the resulting location is shown in Fig. 4. If the 5 GHz detection is real, and the nuclear X-ray emission is smaller by a factor of 2 than the upper limit, then

NGC 821 is consistent with the plane, and it may host a radiatively inefficient accretion flow + jet system. If instead the X-ray emission is close to that of the whole S2 source, or even higher (see Sect. 3.7), then this nucleus lies well below the predictions of the plane. In this case, its SED could be consistent with that of a classical, bright AGN (see Sect. 3.7 below).

The sample of Merloni et al. includes mostly objects of relatively high $L_X = L_{Edd}$. Below a critical $L_X = L_{Edd} \cdot 10^{-5}$, the jet emission can become dominant also in the X-ray domain, and the radio-X-ray correlation should turn steeper (Yuan & Cui 2005). The slope of the fundamental plane should then be different from when the X-ray emission is dominated by the accretion flow (see also Wang et al. 2006), and the fundamental plane in this regime becomes $\log L_R = 1.23 \log L_X + 0.25 \log M_{BH} - 13.45$ (using the radio at 8.5 GHz, Yuan & Cui 2005). This relation predicts a lower radio luminosity for given X-ray emission and therefore the location of the nucleus of NGC 821 is in a better agreement with such a plane (Fig. 4), again provided that the radio emission is close to the 4.2 detection (Sect. 2.1) and the X-ray emission close to the 3 upper limit in Tab. 2.

In conclusion, a radiatively inefficient flow coupled to a nuclear jet is a viable scenario for the accretion process. Also the observed spectral shape of the nuclear source in the radio is consistent with this interpretation. The flux density of a jet with optically thick core/nozzle emission is approximately at $(S / S_{\text{radio}})^{1/2}$ (with $\beta = 0$) up to high radio frequencies (Zensus 1997, Falcke et al. 2004). Within the uncertainties due to the marginal detections at 4.8 and 8.4 GHz and the unattenuated beam widths at the different frequencies (Sect. 2.1), the radio spectral shape of the nuclear source is relatively flat, and is therefore consistent with being produced by the base of a jet. This jet could be confined within the S2 region (of radius 200 pc , Tab. 2), because it is disrupted or frustrated within it; nuclei with parsec-scale jets have already been found in elliptical galaxies with the VLBI (e.g., Nagar et al. 2005).

In the next Section we examine whether a jet/outflow can be present on a larger scale (outside S2).

3.5. A resolved jet?

The elongated X-ray sources S1 and S4 in the central galactic region (P06, Fig. 2) may be due to an outflow or a jet; in the radio, only S2 is detected, but at the location of sources S1 and S4 we could place 4 upper limits (Sect. 2.1). We use here the observed X-ray to radio flux ratios for typical jets to investigate whether S1 and S4 can be due to a jet (note however that the properties of jet emission depend on the internal jet structure as well as the environment in which the jet propagates). Kataoka & Stawarz (2005) compiled a sample of X-ray jets with Chandrasekhar data. They considered X-ray jets observed outside the host galaxy of quasars and AGN. The X-ray luminosity usually dominates over the radio for the jet/knots emission, while for lobes and hot spots the radio luminosity is comparable to or exceeds the X-rays. In any case, in the Kataoka & Stawarz (2005) sample the X-ray to radio $L_{1\text{keV}} / L_{5\text{GHz}}$ monochromatic luminosities ratio does not exceed 100. This sample ratio is > 552 for the source S1, and > 375 for S4, assuming that the entire X-ray luminosity of each source is due to a jet,

and the 4 upper limits at 5 GHz (Sect. 2.1). However, if the observed X-ray luminosity is contributed by several blended knots then the limits quoted above are not meaningful. The case for unresolved knots in sources S1 and S4 is better investigated with more nearby objects. One example of a nearby jet moving within the interstellar medium of a galaxy is the jet of Centaurus A, with many resolved X-ray knots (Hardcastle et al. 2003, Kataoka et al. 2006). Cen A is at 3.4 Mpc distance, so that 1⁰⁰ is equivalent to 17 pc. The size of source S1 (Tab. 3) corresponds to 600 pc, and it is feasible for a jet to create many knots on that distance, given the large number of knots observed in the Cen A jet. Also, for a few knots in the Cen A jet the X-ray to radio luminosity ratio exceeds 100, with one case of > 500 (Hardcastle et al. 2003). The lowest detected 5 GHz luminosity of a radio knot in the Cen A jet is $1.4 \cdot 10^{35}$ erg s⁻¹, which is below our 4 upper limit at 5 GHz of $2.7 \cdot 10^{35}$ erg s⁻¹.

The available radio and X-ray data, although very deep, do not provide therefore a definite conclusion on the jet presence outside the S2 region.

Note that our current data do not resolve the nuclear S2 source, whose X-ray and radio luminosities are measured for a region of 200 pc radius, and could also be related to a small jet. However, the radio spectrum of S2 ($\alpha = 0.33$, Sect. 2.1) does not have the typical slope observed for extragalactic jets or hot spots ($\alpha = 0.6 - 0.8$, Kataoka & Stawarz 2005), but is instead more similar to that of radio-loud AGNs (Elvis et al. 1994), and therefore more likely produced by the base of a jet (as also concluded in Sect. 3.4).

If present, the launch of a nuclear jet/outflow could account for a non-negligible fraction (of the order of a few percent) of the energy associated with the rest mass of the material being accreted (i.e., of $M_{\text{in}} c^2$), as shown to be the case for M 87 (Di Matteo et al. 2003), IC 1459 (Fabbiano et al. 2003) and IC 4296 (Pellegrini et al. 2003) and recently in a few other hot gas rich sources (Allen et al. 2006). This may be a characteristic of the late stages of galaxy evolution, when accretion onto the MBH falls below the Eddington rate (e.g., Churazov et al. 2005). Unfortunately, radio synchrotron emission traces poorly the true jet power (Owen et al. 2000, Bazzan et al. 2004), with the ratio of the mechanical (kinetic) luminosity to the 1.4 GHz synchrotron luminosity ranging between a few and roughly a few thousand for luminous radio sources, and up to several thousand for weaker sources. Notwithstanding these uncertainties, in this case the jet kinetic power could account for a few 10^4 of $M_{\text{in}} c^2$, for the nuclear radio source coincident with S2 and detected at 1.4 GHz, and at most this fraction for the S1 and S4 sources with upper limits at 1.4 GHz. To increase this fraction, one should suppose that an injection of energy from the nucleus is heating the surroundings, so that accretion has been recently stopped or is lowered to values below the M_{in} estimated in the numerical simulations of P06 that do not include feedback (Sect. 3.1; e.g., Di Matteo et al. 2003, Ciotti & Ostriker 2001).

3.6. Disk instability

The mode of accretion may switch to a quiescent state due to the change in internal structure of the accretion flow produced by disk instabilities (Sienigunowka et al.

1996, Janiuk et al. 2004), with the time scale in the low quiescent state longer than that in the active state. In such a case the accretion flow can be described by a hybrid model, where an outer torus or cold disk accumulates accreting matter at the steady accretion rate, while the inner torus/disk has a low accretion rate and is radiatively inefficient. The transition radius between the two regions is set by the hydrogen ionization instability and depends on the accretion conditions onto the outer torus.

For the MBH mass of NGC 821 (Tab. 1) the gravitational radius is located at $R_g = 2.5 \cdot 10^{13}$ cm. Assuming an accretion rate of $2 \cdot 10^{-5} M_{\odot} \text{ yr}^{-1}$ (Sect. 3.1), the location of the ionization zone is at $100R_g$ (Janiuk et al. 2004). In the hybrid model we expect the outer disk to be cold and to emit a thermal spectrum with a total disk luminosity for these parameters of about $2.5 \cdot 10^{37}$ ergs sec⁻¹, that will be radiated mainly in the optical and near IR bands. This value is well within the observed limits (Tab. 5 and Fig. 3). The X-ray luminosity will come from the inner quasi-spherical accretion flow and depend on the density and temperature of the plasma; its value needs to be self-consistently calculated, which is beyond the scope of this work (it is the subject of Moscibrodzka et al., in preparation).

3.7. A standard AGN (but very obscured)

We examine here the possibility that the nucleus of NGC 821 is a normal AGN working at a very sub-Eddington rate ($L_{\text{acc}} = L_{\text{Edd}} \text{ few } 10^{-5}$, with L_{acc} estimated for a standard disc as described in Sect. 3.1), and test this hypothesis using the whole observed SED (Fig. 3). L_{acc} is 30 (100) times larger than the upper limit on L_{bol} of pointlike nuclear emission (for a bolometric correction of $L_{\text{bol}} = 20L_{\text{2 keV}}$, Elvis et al. 1994). We consider then the possibility that the X-ray radiation is heavily absorbed, so that the intrinsic L_{bol} is comparable to L_{acc} .

A Compton thin AGN with $N_H = 10^{23-24}$ cm⁻² (e.g., Bassani et al. 1999) can be excluded, since the X-ray spectrum of S2 does not show the characteristic cut-off at low energies (Tab. 2). A more interesting possibility is that S2 is a Compton thick AGN, where the direct nuclear emission is not detectable below 10 keV because of an absorber of very large column density ($N_H > 10^{24}$ cm⁻²; e.g., Guainazzi et al. 2005). However, some few percent of the intrinsic emission is often scattered and reprocessed or some Compton thick 'mirror' visible both to us and from the central continuum source, and may emerge below 10 keV with a flatter photon index than the intrinsic X-ray continuum (i.e., with $\alpha = 1$), as for example in the Circinus galaxy (Matt et al. 1999). The resulting X-ray spectrum also shows a very strong (equivalent width & 1 keV) iron K⁺ fluorescent line (as in NGC 1068, Levenson et al. 2006). S2 has quite a flat spectral shape ($\alpha = 1.49^{+0.14}_{-0.13}$), reminiscent of what is found for Compton-thick sources; a 6.4 keV iron line is not seen in its X-ray spectrum, but only with a 1 upper limit on its equivalent width of 2 keV (Tab. 2). Note also that extended emission has been observed associated with some obscured Seyfert nuclei, up to sizes of 1 kpc (Elvis et al. 1990, Ogle et al. 2000), and is understood as emission from gas photoionized by the central AGN, or

thermalem ission from a hot collisionally ionized plasm a that form s the intercloud medium . Therefore, this X-ray faint M BH m ay be an extreme scaled-down version of such obscured AGNs, and the extended S2 source could be nuclear ux scattered and uorescing o cold gas. Evidence for Seyfert nuclei (including Compton-thick ones) being scaled-down versions of more luminous AGNs down to 2{10 keV luminosities of 10^{39} erg s⁻¹ has been provided recently (Panessa et al. 2006), based on the significance of the correlation between $L_{2-10\text{keV}}$ and $L(H)$ down to such low X-ray luminosity values. This implies a similar proportion of X-ray and UV ionizing radiation in high and low luminosity nuclei, so that the shape of their SEDs m ay be similar in these spectral regions.

If we assume that a typical 1% of the intrinsic AGN ux is scattered into our line of sight and observed as source S2 with a $L(2-10\text{keV}) = 4 \times 10^{38}$ erg s⁻¹ (Tab. 2), the intrinsic $L_{\text{bol}} = 8 \times 10^{41}$ erg s⁻¹ for a standard AGN SED (Elvis et al. 1994), a luminosity that is consistent with L_{acc} . L_{bol} could be even higher, since some nearby AGN show < 1% of their X-ray ux scattered, perhaps due to the lack of an appropriately positioned 'mirror' (NGC 4051, Uttley et al. 2003). An intrinsic 2{10 keV luminosity as large as assumed here would place the NGC 821 nucleus way o the fundamental plane of Sect. 3.4 (increasing its x-axis value of 1.4 in Fig. 4), consistent with the hypothesis of a standard disc rather than a radiatively inefficient accretion flow.

How does this hypothesis of the nucleus of NGC 821 being a scaled-down, highly obscured AGN compare with the available observational constraints?

The intrinsic SED w ould have the typical AGN shape of Elvis et al. (1994) shown in Fig. 3, rescaled up by a factor of 200 for a 1% re ectance (since the average AGN SED in Fig. 3 is normalized to the upper limits on pointlike X-ray emission in Tab. 2, that are 2 times lower than the S2's luminosities). The upper limits in the V and I bands allow for this shift, but the NICMOS F160W band limit lies just a factor 10 above both the radio-quiet and radio-loud SEDs before rescaling. Even though the dispersion in the SEDs of a AGN is rather large (even an order of magnitude in the X-ray to optical+UV ratio, Risaliti & Elvis 2004), scaling up the optical+IR SED of NGC 821 by only a factor of 10 and the X-rays by a factor of 200 w ould produce an α_X index of -1 , that is de nitely too low with respect to what typically observed (Risaliti & Elvis 2004). Therefore, a hidden AGN m ay have a 20% re ectance, rather than 1% as assumed above, and then $L_{\text{bol}} = 4 \times 10^{40}$ erg s⁻¹. This L_{bol} is a factor of 2 lower than L_{acc} , which could be explained by a similarly lower radiative e ciency (with respect to the standard value of 0.1 used in Sect. 3.1) and/or by M_{in} being lower (due, e.g., to angular momentum in the flow before being captured by the M BH, Sect. 3.2, or to a heating source, Sect. 3.5). With a 20% re ectance, and the H upper limit of Sect. 3.3, this nucleus w ould lie close to the $L(2-10\text{keV})/L_H$ correlation (Panessa et al. 2006), at higher X-ray luminosities with respect to the best t line but well within the observed scatter.

Another observational constraint comes from the fact that thermal reradiation of an obscured continuum should appear as dust emission in the IR. The IRAC data

in Fig. 3 t very well to the SED of a stellar population (Sect. 3.3), so that any warm /hot dust m ust be negligible. The 8 m ux (Tab. 5) corresponds to 3.4×10^{40} erg s⁻¹, and any fraction due to dust m ust be much less than this. A conservative limit w ould be that the dust ux is less than the difference of the uxes at 8 m and 5.8 m , otherwise the SED w ould depart from the galaxy template. That difference (0.5 m Jy, from Tab. 5) corresponds to a luminosity limit of $< 3.1 \times 10^{40}$ erg s⁻¹, that is a factor of 10 less than L_{acc} . The prevalence of a non-nuclear origin for the Spitzer IRAC measurements, that refer to an area of 4 square arcseconds, is indicated also by a color analysis. Spitzer IRAC colors have been shown to provide a robust technique for identifying AGNs, i.e., inactive galaxies can be separated from AGNs in a [3.6]{[4.5]} versus [5.8]{[8.0]} plot (Stern et al. 2005). We calculated such colors (in the Vega system) for the nucleus of NGC 821, using uxes derived with a local background in order to better single out the nuclear emission (Tab. 4), and found that it falls well within the region of normal galaxies. This means that stars within the central 1 '' radius dominate over the IR nuclear emission (Sect. 3.3). Longer wavelength data are crucial to de nitely rule out the possibility of heavily obscured emission. Unfortunately, NGC 821 has not been detected by IRAS (Knap et al. 1989)⁸. Spitzer MIPS imaging has been scheduled and, possibly together with deeper HST/NICMOS F160W images, should be useful to de nitely test the hypothesis of a hidden AGN .

4. SUMMARY AND CONCLUSIONS

NGC 821 is an extreme example of a quiescent M BH, for which deep Chandra and VLA observations revealed an extremely sub-Eddington nuclear source for the first time. Since NGC 821 is relatively nearby, it is a good testcase to study how accretion proceeds in the very low luminosity galactic nuclei that are the vast majority in the local universe (e.g., Ho 2005, Pellegrini 2005). Our multiwavelength analysis has shown that:

1. A radio counterpart to the Chandra nuclear source S2 is detected at 1.4 GHz, with a ux density of 127 mJy. A source is also marginally (4 level) detected at 4.8 and 8.4 GHz. Within current uncertainties, the radio spectral shape of the nuclear source is relatively flat. Upper limits can be placed at the positions of the other elongated Chandra sources in the central galactic region (S1 and S4).
2. The central 1 '' radius region is also detected with Spitzer IRAC, with the emission peak coincident with the position of the galactic center. Archival HST images taken with W FPC 2/F555W, W FPC 2/F814W and NICMOS (H-band) do not show a pointlike source at the galactic center.
3. A dead M BH could be expected from the lack of detection of fuel at all wavelengths. However, the stellar mass losses in the circum nuclear region should produce a luminosity of L_{acc} few 10^{41} erg s⁻¹.

⁸ With IRAS data just an uncertain 1 detection of 0.5 Jy at 100 m could be placed [J. Knap 1994, private communication to NED (<http://nedwww.ipac.caltech.edu/>)], corresponding to 10^{42} erg s⁻¹.

s^{-1} , if they end in a standard disc (such a scaled-down AGN would work at $L_{acc}=L_{Edd}$ few 10^5).

4. Disc-like stellar kinematics in the central galactic region, with the consequent angular momentum of the accretion flow at large radii, may account for a reduction of the mass accretion rate; MHD simulations with rotation and cooling by radiation included are needed to estimate the nuclear ionosity of the flow.

5. Starformation in the accreting material could also reduce the actual fuel supply to the MBH. The mid-IR to V-band photometric data for a central 1° radius, though, are very well fitted by the spectral energy distribution of an old and metal rich stellar population. High angular resolution optical spectral indices also do not reveal current starformation.

6. The upper limit on pointlike $2-10$ keV nuclear emission, together with the 5 GHz (4.0) and 8.4 GHz (4.2) detections, and the MBH mass known from HST data, are consistent with the predictions for radiatively inefficient accretion coupled to a compact, nuclear jet. The relatively flat radio spectral shape of the nuclear source is also consistent with that of the base of a jet.

7. The extended Chandra sources S1 and S4, close to the nucleus, could be due to several knots in a jet, since their X-ray to radio luminosity ratios are not too far from those observed for the knots in the Cen A jet; more sensitive radio observations are needed to draw final conclusions on this possibility. The mechanical energy possibly associated with the nuclear jet or the resolved jets would be a very small fraction (a few 10^{-4}) of the energy associated with the rest mass of the material being accreted, where the latter is estimated by numerical simulations not including feedback.

8. The nucleus of NGC 821 could be a standard AGN working at $L_{acc}=L_{Edd}$ few 10^5 and heavily obscured as in a Compton-thick source, possibly also extended as S2 is. The N ICMOS upper limit on the nuclear emission constrains the re-estimate in the X-rays, but plausibly the intrinsic L_{bol} could be of the order of L_{acc} . Thermal re-radiation by dust is expected in the obscured scenario. The possible presence of warm/hot dust is strongly constrained by the Spitzer mid-IR data; far-IR observations are needed to estimate the emission from cold dust.

In conclusion, the nucleus of NGC 821 has proved to be a very interesting object, since it shows that MBHs in the local universe are still emitting, though at an extremely low level, even in low L_B ellipticals, that are expected to be very poor (or devoid) of hot gas. This supports the finding of hydrodynamical simulations that stellar mass losses in the circumnuclear region can fuel the MBH, even in low L_B galaxies, though at a very low level. The multiwavelength study of this nucleus shows that the final stages of accretion could be radiatively inefficient and possibly coupled to a compact nuclear jet/outflow. A standard disc in a Compton-thick (scaled-down) AGN cannot be excluded, provided that the radiative efficiency and/or the mass accretion rate are reduced by a small factor, which does not seem unlikely. Deeper N ICMOS and radio observations, together with far-IR data, are expected to shed more light on the nature of the accretion process in this intriguing nucleus.

We warmly thank M. Bolzonella for providing the fitting SEDs for Sect. 3.3. S.P. acknowledges financial support from ASI (Agenzia Spaziale Italiana) contract I/023/05/0. Partial support for this work was provided by the NASA Chandra Guest Observer grant GO 5-6110X and by the Chandra X-ray Center NASA contract NAS8-39073 and by the Spitzer Cycle-2 program 20371. The data analysis was supported by the CXO CIAO software and CALDB. We have used NASA NED and ADS facilities, and have extracted archival data from the Hubble Space Telescope archive.

REFERENCES

Allen, S.W., Dunn, R.J.H., Fabian, A.C., Taylor, G.B., Reynolds, C.S. 2006, MNRAS, in press

Anderson, J.M., Uvestad, J.S., Ho, L.C. 2004, ApJ 603, 42

Balbus, S.A., Hawley, J.F. 2002, ApJ 573, 749

Bassani, L., D'Adina, M., Maiolino, R., Salvati, M., Risaliti, G., Della Ceca, R., Matt, G., Zamorani, G. 1999, ApJS 121, 473

Bazzan, L., Raftery, D.A., McDonald, B.R., Wise, M.W., Nulsen, P.E.J. 2004, ApJ 607, 800

Blandford, R.D., Begelman, M.C. 2004, MNRAS 349, 68

Bolzonella, M., Miralles, J.M., Pello, M. 2003, A&A 363, 476

Bondi, H. 1952, MNRAS, 112, 195

Bruzual, G., Charlot, S. 2003, MNRAS 344, 1000

Churazov, E., Sazonov, S., Sunyaev, R., Forman, W., Jones, C., Böhringer, H. 2005, MNRAS 363, L91

Cioffi, L., D'Ecole, A., Pellegrini, S., Renzini, A. 1991, ApJ 376, 380

Cioffi, L., & Ostriker, J.P. 2001, ApJ, 551, 131

Coron, D.J., Springel, V., White, S.D.M., et al. 2006, MNRAS 365, 11

David, L.P., Forman, W., Jones, C. 1991, ApJ 369, 121

de Vaucouleurs, G., de Vaucouleurs, A., Corwin, Jr., H.G., Buta, R.J., Paturel, G., Fouque, P., 1991, Third Reference Catalogue of Bright Galaxies, (New York: Springer Verlag) (RC3)

De Viliers, J.-P., Hawley, J.F., & Krolik, J.H. 2003, ApJ, 599, 1238

Dickey, J.M., Lockman, F.J. 1990, ARA&A 28, 215

Dimatteo, T., Allen, S.W., Fabian, A.C., Wilson, A.S., & Young, A.J. 2003, ApJ, 582, 133

Elvis, M., Fassnacht, C., Wilson, A.S., Briel, U. 1990, ApJ 361, 459

Elvis, M., Wilkes, B.J., McDowell, J.C., et al. 1994, ApJS 95, 1

Elvis, M., Risaliti, G. 2004, Supermassive Black Holes in the Distant Universe, Amy J. Barger ed., Kluwer Academic Publishers, Dordrecht, The Netherlands, p.187

Emsellem, E., Cappellari, M., Peletier, R.F., et al. 2004, MNRAS 352, 721

Fabbiano, G., Elvis, M., Markoff, S., Siemiginowska, A., Pellegrini, S., Zezas, A., Nicastro, F., Trinchieri, G., & McDowell, J. 2003, ApJ 588, 175

Fabbiano, G., Baldi, A., Pellegrini, S., Siemiginowska, A., Elvis, M., Zezas, A., & McDowell, J. 2004, ApJ, 616, 730

Fabian, A.C., & Canizares, C.R. 1988, Nature, 333, 829

Fabian, A. C., Sanders, J. S., Taylor, G. B., Allen, S. W., Crawford, C. S., Johnstone, R. M., Iwasawa, K. 2006, *MNRAS* 366, 417

Falcke, H., Koerding, E., Marko, S. 2004, *A&A* 414, 895

Fazio, G. G., Hora, J. L., Allen, L. E., et al. 2004, *ApJS* 154, 10

Ferrarese, L., Merritt, D. 2000, *ApJ* 539, L9

Ferrarese, L., Ford, H. 2005, *Space Science Reviews* 116, 523

Gebhardt, K., Bender, R., Bower, G., et al. 2000, *ApJ* 539, L13

Gebhardt, K., Richstone, D., Tremaine, S., et al. 2003, *ApJ* 583, 92

Graham, A. W., Erwin, P., Caon, N., & Trujillo, I. 2001, *ApJ*, 563, L11

Guainazzi, M., Fabian, A. C., Iwasawa, K., Matt, G., Fiore, F. 2005, *MNRAS* 356, 295

Hardcastle, M. J., Worrall, D. M., Kraft, R. P., Forman, W. R., Jones, C., & Murray, S. S. 2003, *ApJ* 593, 169

Hawley, J. F., & Balbus, S. A. 2002, *ApJ*, 573, 738

Ho, L. C. 2002, *ApJ* 564, 120

Ho, L. C., Filippenko, A. V., Sargent, W. L. W. 2003, *ApJ* 583, 159

Ho, L. C. 2005, *Ap&SS* 300, 219

Hopkins, P. F., Hemquist, L., Cox, T. J., Di Matteo, T., Robertson, B., Springel, V. 2006a, *ApJS* 163, 1

Hopkins, P. F., Narayan, R., Hemquist, L. 2006b, *ApJ* 643, 641

Janiuk, A., Czerny, B., Siemiginowska, A., & Szczepański, R. 2004, *ApJ* 602, 595

Igumenshchev, I. V., Narayan, R., Abramowicz, M. A. 2003, *ApJ* 592, 2042

Kataoka, J., Stawarz, L. 2005, *ApJ*, 622, 797

Kataoka, J., Stawarz, L., Aharonian, F., Takahara, F., Ostriwski, M., Edwards, P. G. 2006, *ApJ*, 641, 158

Kennicutt, R. C. 1998, *ARA&A* 36, 189

Knap, G. R., Guhathakurta, P., Kim, D.-W., Jura, M. A. 1989, *ApJS* 70, 329

Kording, E. G., Jester, S., Fender, R. 2006, *MNRAS* 372, 1366

Kroupa, P. 2001, *MNRAS* 322, 231

Lauer, T. R., et al. 2005, *AJ* 129, 2138

Loewenstein, M., Moshotzky, R. F., Angelini, L., Amund, K. A., & Quataert, E. 2001, *ApJ*, 555, L21

Levenson, N. A., Heckman, T. M., Kralik, J. H., Weaver, K. A., Zyci, P. T. 2006, *ApJ* 648, 111

Machacek, M., Nulsen, P. E. J., Jones, C., Forman, W. R. 2006, *ApJ* 648, 947

Matt, G., Guainazzi, M., Maiolino, R. et al. 1999, *A&A* 341, L39

McNamara, B. R., Nulsen, P. E. J., Wise, M. W., Raftery, D. A., Carilli, C., Sarazin, C. L., Banton, E. L. 2005, *Nature* 433, 45

Merloni, A., Heinz, S., Di Matteo, T. 2003, *MNRAS* 345, 1057

Moscibrodzka, M. 2006, *A&A* 450, 93

Nagar, A., Falcke, H., Wilson, A. S. 2005, *A&A* 435, 521

Narayan, R. 2005, *Ap&SS* 300, 177

Ogle, P. M., Marshall, H. L., Lee, J. C., Canizares, C. R. 2000, *ApJ* 545, 81

Omega, H., Binney, J., Bryan, G., & Slyz, A. 2004, *MNRAS*, 348, 1105

Stricker, J. P., Ciotti, L. 2005, *RSPTA* 363, 667

Owen, F. N., Eilek, J. A., Kassim, N. E. 2000, *ApJ* 543, 611

Panessa, F., Bassani, L., Cappi, M., Adina, M., Barcons, X., Carrera, F. J., Ho, L. C., Iwasawa, K. 2006, *A&A* 455, 173

Pellegrini, S., Venturi, T., Comastri, A., Fabbiano, G., Fiore, F., Vignali, C., M. organi, R., Trinchieri, G. 2003, *ApJ* 585, 677

Pellegrini, S. 2005a, *ApJ*, 624, 155

Pellegrini, S. 2005b, *MNRAS* 364, 169

Pellegrini, S., Baldi, A., Kim, D. W., Fabbiano, G., Soria, R., Siemiginowska, A., Elvis, M. 2006, submitted to *ApJ* (P06)

Pinkney, J., Gebhardt, K., Bender, R., et al. 2003, *ApJ* 596, 903

Proctor, R. N., Forbes, D. A., Forestell, A., Gebhardt, K. 2005, *MNRAS* 362, 857

Pogosyan, D., Begelman, M. C. 2003, *ApJ* 592, 767

Ravindranath, S., Ho, L. C., Peng, C. Y., Filippenko, A. V., Sargent, W. L. W. 2001, *AJ* 122, 653

Sarzi, M., Falcon-Barroso, J., Davies, R. L., et al. 2006, *MNRAS* 366, 1151

Sazonov, S. Yu., Stricker, J. P., Ciotti, L., Sunyaev, R. A. 2005, *MNRAS*, 358, 168

Schlegel et al. 1998, *ApJS* 500, 525

Scorza, C., Bender, R. 1995, *A&A* 293, 20

Shakura, N. J., & Sunyaev, R. A. 1973, *A&A*, 24, 337

Siemiginowska, A., Czerny, B., Kostryukin, V. 1996, *ApJ* 458, 491

Soria, R., Fabbiano, G., Graham, A., Baldi, A., Elvis, M., Jerjen, H., Pellegrini, S., Siemiginowska, A. 2006a, *ApJ* 640, 126

Soria, R., Graham, A., Fabbiano, G., Baldi, A., Elvis, M., Jerjen, H., Pellegrini, S., Siemiginowska, A. 2006b, *ApJ* 640, 143

Springel, V., Di Matteo, T., Hemquist, L. 2005, *ApJ* 620, L79

Stem, D., Eisenhardt, P., Gorjian, V., et al. 2005, *ApJ* 631, 163

Stone, J. M., Pringle, J. E., Begelman, M. C. 1999, *MNRAS* 310, 1002

Tan, J., Blackman, E. 2005, *MNRAS* 362, 983

Terashima, Y., Wilson, A. S. 2003, *ApJ* 583, 145

Tonry, J. L., Dressler, A., Blakeslee, J. P., et al. 2001, *ApJ*, 546, 681

Uttley, P. et al. 2003, *ApJ* 595, 656

Wang, R., Wu, X.-B., Kong, M.-Z. 2006, *ApJ* 645, 890

Werner, M. W., Roellig, T. L., Low, F. J., et al. 2004, *ApJS* 154, 1

Wobel, J. M., Heeschen, D. S. 1991, *AJ* 101, 148

Wu, Q., Cao, X. 2005, *ApJ* 621, 130

Yuan, F., Cui, W. 2005, *ApJ* 629, 408

Zensus, J. A. 1997, *ARA&A* 35, 607

TABLE 1
NGC 821: main properties

Type ^a	B_T^0 ^a (mag)	D ^b (Mpc)	$\log L_B$ (L_B ,)	Size ^a (arcmin)	R_e ^c (0 , kpc)	v_e ^d (km s ⁻¹)	N_H ^e (cm ⁻²)	M_{BH} ^f ($10^7 M_\odot$)	100 (pc)
E6	11.72	24.1	10.27	2.57x1.62	43.9, 5.1	209	6.2 10^{20}	8.5 3.5	117

^a Type, B_T^0 and size from de Vaucouleurs et al. (1991; RC 3). The size gives the major and minor axis of the D 25 ellipse, that is the 25.0 B-mag/square arcsec isophote. The position angle is 25 (RC 3).

^b Distance D from Tonry et al. (2001).

^c Effective radius R_e in the R-band (from Soria et al. 2006b).

^d Effective stellar velocity dispersion (averaged over R_e) from Pinkney et al. (2003).

^e Galactic hydrogen column density (Dickey & Lockman 1990).

^f Gebhardt et al. (2003) report a value of $3.7^{+2.4}_{-0.8} \cdot 10^7 M_\odot$, later revised to the value given here (Richstone et al., astro-ph/0403257) that is considered more reliable (Gebhardt, K. 2006, private communication).

TABLE 2
The Chandra source S2

Position (J2000) :	RA	Dec
HST (galactic center)	02 ^h 08 ^m 21 ^s 13	+ 10 59 ⁰ 41 ⁰ 8
Chandra	02 ^h 08 ^m 21 ^s 10	+ 10 59 ⁰ 41 ⁰ 6
VLA	02 ^h 08 ^m 21 ⁰ 174	+ 10 59 ⁰ 41 ⁰ 4
Spitzer	02 ^h 08 ^m 21 ^s 11	+ 10 59 ⁰ 42 ⁰ 0
Size of ellipse ^a	1 ⁰ 7	1 ⁰ 5
Spectral analysis of Chandra data:		
Net counts ^b	246	16
Model w abs (pow) :		
N _H (10 ²¹ cm ⁻²)	< 0.5	
	1.49 ^{+0.14} _{-0.13}	
² =dof	11.5/9	
L (0.3{8 keV})/10 ³⁸ erg s ⁻¹	6.0	
L (2{10 keV})/10 ³⁸ erg s ⁻¹	3.8	
Model w abs (pow + gauss) ^c :		
N _H (10 ²¹ cm ⁻²)	< 0.5	
	1.55 ^{+0.14} _{-0.17}	
EW (keV)	0.9 (< 2.0)	
² =dof	11.2/8	
L (0.3{8 keV})/10 ³⁸ erg s ⁻¹	6.3	
L (2{10 keV})/10 ³⁸ erg s ⁻¹	5.0	
Pointlike emission ^d within S2:		
L (0.3{8 keV})/10 ³⁸ erg s ⁻¹	< 2.8	
L (2{10 keV})/10 ³⁸ erg s ⁻¹	< 1.8	

^a Length of semi major and semi minor axes of the ellipse describing the source shape, derived by the CIAO task wavdetect (P06).

^b From a total net exposure time of 226 ksec.

^c The energy of the gaussian emission line has been fixed at 6.4 keV.

^d Calculated as described in P06.

Note. | The column density N_H is in addition to the Galactic one (see P06). Errors give the 68% confidence interval for one interesting parameter.

TABLE 3
The *Chandra* sources S1 and S4

	S1		S4	
Size (ellipse) ^a	2 ^{0.5}	1 ^{0.5}	1 ^{0.2}	1 ^{0.0}
Net counts ^b	178	14	82	9
M odel w abs (pow) :				
N _H (10 ²¹ cm ⁻²)	1.7 ^{+0.8} 1.0	3.0 ^{+1.3} 1.5	2.28 ^{+0.52} 0.34	
χ^2_{ν}	7.3/6	2.1/5		
L (0.3-8 keV)/10 ³⁸ erg s ⁻¹	4.7	1.9		

^a Length of semi-major and semi-minor axes of the ellipse describing the source shape, derived by the CIAO task wavdetect (P06).

^b From a total net exposure time of 226 ksec.

Note. | The column density N_H is in addition to the Galactic one (see P06). Errors give the 68% confidence interval for one interesting parameter.

TABLE 4

Spitzer fluxes from an area of 4 square arcseconds centered on the nucleus of NGC 821.

Band	Flux density (m Jy)		Flux density (m Jy)	
	local bkgd	eld bkgd	local bkgd	eld bkgd
3.6 m	2.4	0.5	5.6	0.5
4.5 m	1.1	0.4	3.1	0.4
5.8 m	0.7	0.2	1.8	0.2
8 m	0.4	0.3	1.3	0.2

Fluxes are given for two choices of the background: estimated from a surrounding annulus (local) and from an off-source circle (eld), see Sect. 2.2.

TABLE 5
Spectral energy distribution of the nucleus of NGC 821.

Band	Flux Density	L (erg s ⁻¹)	Region (°)	Instrument
1.4 GHz	127 Jy	1.2 10^{35}	$R = 1.3$ circle	VLA (Sect. 2.1)
4.8 GHz	(80 Jy) ^a	(2.7 10^{35})	4.1 4.0, (56 deg) ^b	∞
8.4 GHz	(71 Jy) ^a	(4.1 10^{35})	2.7 2.2, ∞	∞
15 GHz	< 1.5 mJy	< 1.5 10^{37}	$R = 0.15$ circle	VLA (5 limit; Nagar et al. 2005)
8 m	1.3 0.2 mJy	3.4 10^{40}	$R = 1.1$ circle	Spitzer IRAC (Sect. 2.2)
5.8 m	1.8 0.2 mJy	6.5 10^{40}	∞	∞
4.5 m	3.1 0.4 mJy	1.4 10^{41}	∞	∞
3.6 m	5.6 0.5 mJy	3.2 10^{40}	∞	∞
1.6 m	< 0.01 mJy ^c	< 1.4 10^{39}	$R = 0.02$ circle	NICMOS (Ravindranath et al. 2001)
I (0.90 m)	7.45 ^{+0.72} _{-0.66} mJy	1.9 10^{42}	$R = 1.1$ circle	WFPC2 F814W (Sect. 2.3)
∞	< 0.19 mJy ^c	< 4.3 10^{40}	$R = 0.046$ circle	∞
R (0.70 m)	5.47 ^{+0.53} _{-0.48} mJy	1.7 10^{42}	$R = 1.1$ circle	INT (Sect. 2.3)
V (0.55 m)	3.54 ^{+0.34} _{-0.31} mJy	1.3 10^{42}	∞	WFPC2 F555W (Sect. 2.3)
∞	< 0.075 mJy ^c	2.8 10^{40}	$R = 0.046$ circle	∞
2.4 10^{17} Hz	< 6.5 10^{-7} ph cm ⁻² s ⁻¹ keV ⁻¹	< 7.2 10^{37}	1 1	Chandra ACIS-S ^d (Sect. 2)
4.8 10^{17} Hz	< 2.0 10^{-7} ph cm ⁻² s ⁻¹ keV ⁻¹	< 8.7 10^{37}	∞	∞
2.4 10^{18} Hz	< 1.3 10^{-8} ph cm ⁻² s ⁻¹ keV ⁻¹	< 1.7 10^{38}	∞	∞

^a The 4.8 GHz is a 4.0 detection, and the 8.4 GHz is a 4.2 detection.

^b Position angle of the beam.

^c Upper limits to any "AGN" flux density (the brightness profile is consistent with that of the normal galactic stellar emission).

^d 3 upper limits on pointlike nuclear emission (P06).

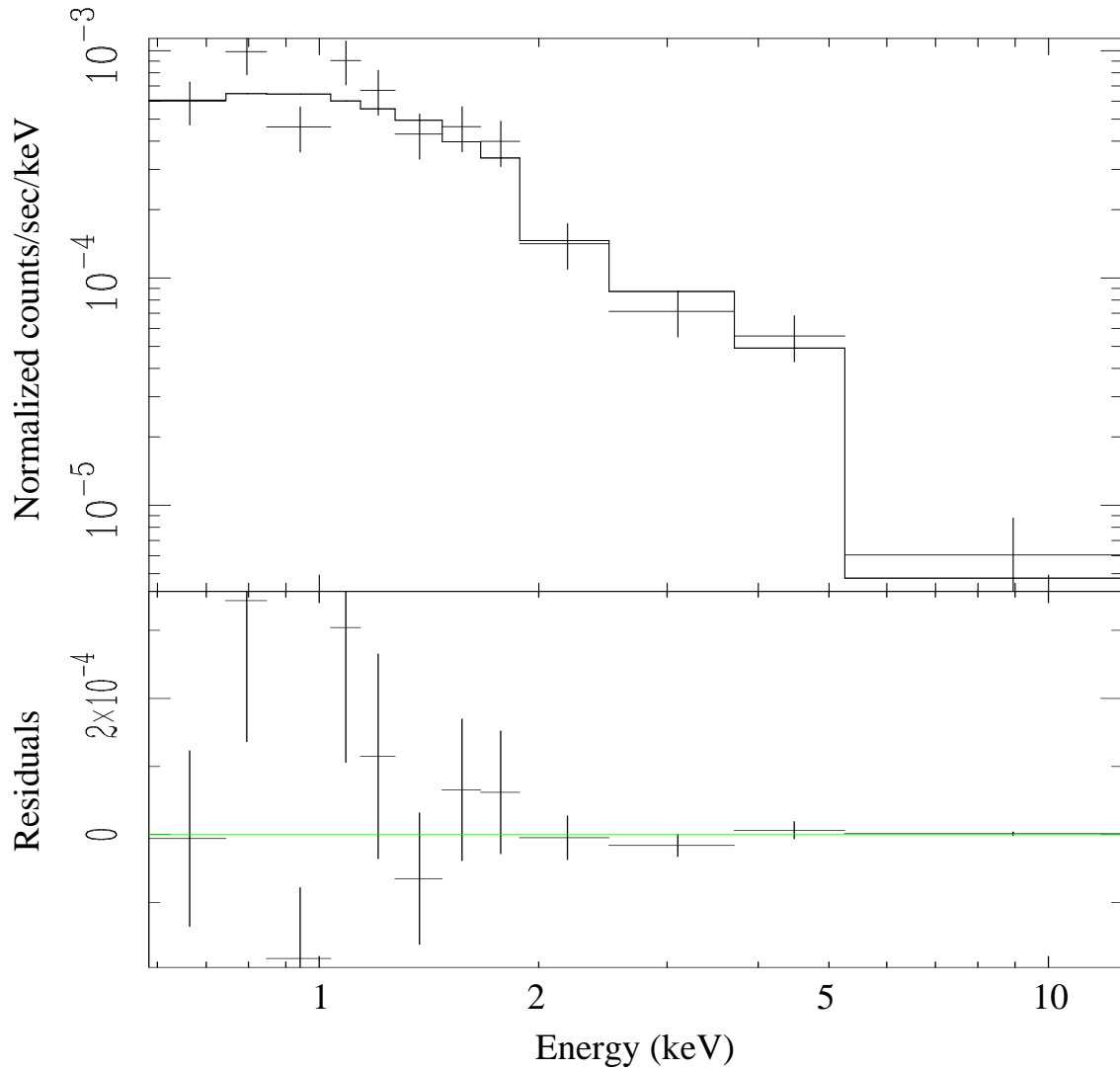


Fig. 1. The Chandra ACIS-S spectrum of the source S2 detected at the center of NGC 821 with the deep pointing (P06). Upper panel: data and best χ^2 power law model; lower panel: the residuals from the best χ^2 (Tab. 2)

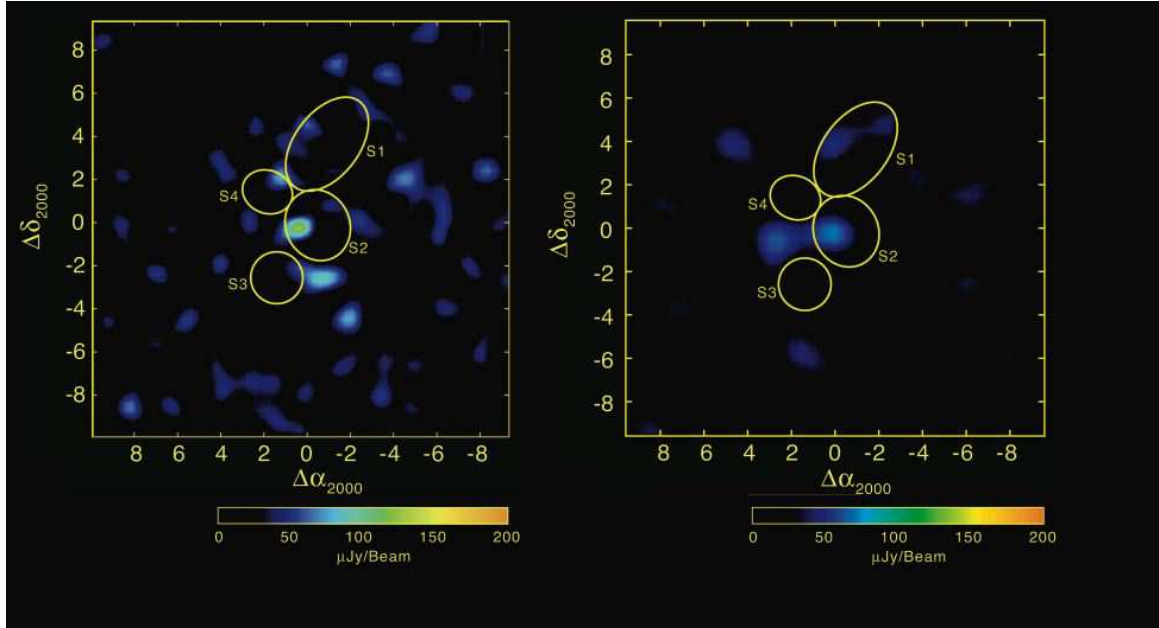


Fig. 2.1 Radio image of the central 17^{00} (~ 2 kpc) of NGC 821 at 1.4 GHz (left) and 8.4 GHz (right). The position and sizes of the ellipses corresponding to the Chandra sources S1-S4 (P 06) are superposed. The beam size was $1^{03} \times 1^{03}$ at 1.4 GHz and $2^{07} \times 2^{02}$ at 8.4 GHz (half-power full width). The coordinate origin is $02^{\text{h}} 08^{\text{m}} 21^{\text{s}}.140, +10^{\circ} 59' 41.70$ (J2000).

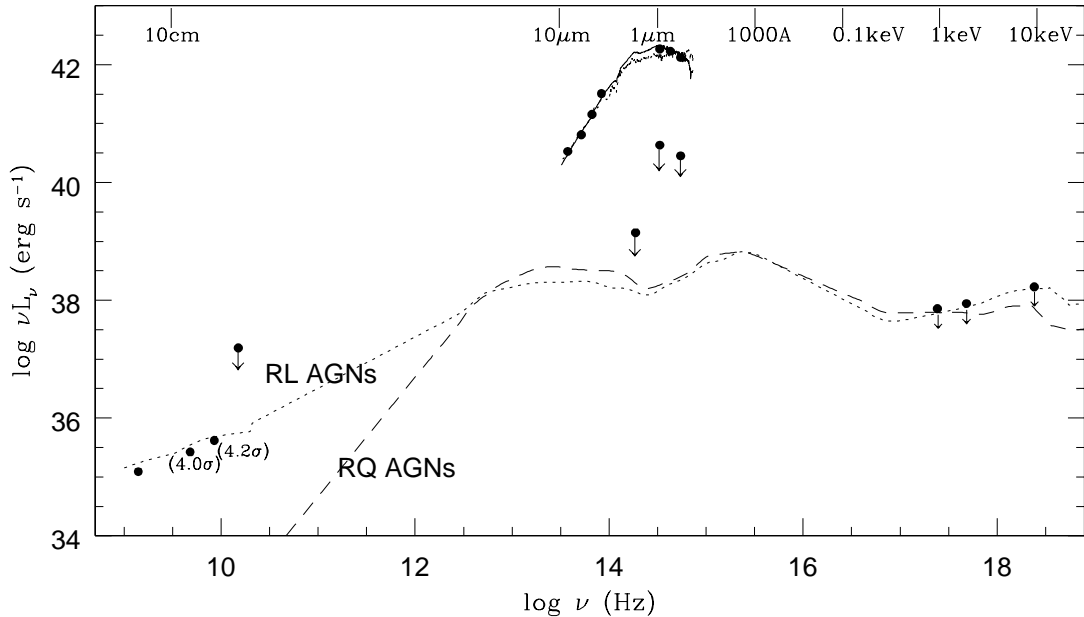


Fig. 3.1| The spectral energy distribution of the nuclear emission of NGC 821 (data in Tab. 5; see also Sect. 2). The radio detection at 1.4 GHz, and the 40 and 42 detections at 4.8 and 8.4 GHz, come from our VLA observations; the 15 GHz upper limit is from Nagar et al. (2005, Sect. 2.1). The Spitzer IRAC measurements from 8 to 3.6 μm derive from our Spitzer observations and refer to a circle of 10' radius (Sect. 2.2) for the field background; the upper limit at 1.6 μm is from NICMOS data (Ravindranath et al. 2001) for a circle of 0''.02 radius. The I, R and V measurements refer to the same extraction area used for the Spitzer data, and derive from our analysis of the HST WFPC2 F814W and F555W image, and of an INT image (Soria et al. 2006b). From these HST images, an upper limit to the nuclear emission (i.e., the luminosity enclosed within 0''.046) has been derived from the deconvolved profile of Lauer et al. (2005, see Sect. 2.3). The 1, 2, 10 keV upper limits refer to a pointlike emission possibly associated with the MBH, from Chandra data (Tab. 2; P06). Dotted and dashed lines show the median distribution observed for low redshift radio loud and radio quiet AGNs (Elvis et al. 1994), rescaled to match the X-ray upper limits. The solid line gives the best fit SED of Bruzual & Charlot (2003) to the Spitzer and I, R, V data (see Sect. 3.3); also shown (dotted line) is the best fit SED for higher abundance and younger age.

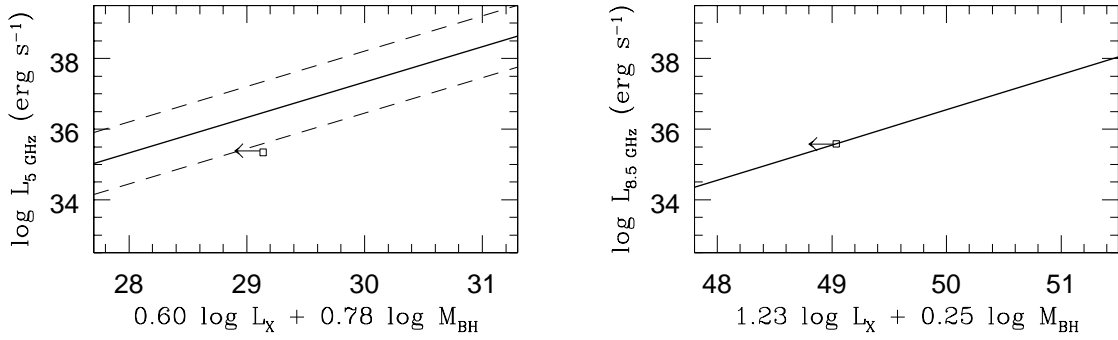


Fig. 4.1 Location of the nucleus of NGC 821 with respect to the fundamental plane of black hole activity. Left: the plane of Merton et al. (2003) is indicated with a solid line, together with the scatter of $\log R = 0.88$ of observed sources (dashed lines); right: the plane of Yuan & Cui (2005). See also Sect. 3.4.